International journal of COMADEM
Vol 24 No 3 (September 2021) p.27-34

COMADEM
International Journal of Condition Monitoring and Diagnostic Engineering Management

A Smart Impact Detection System for Thermoplastic Aircraft Components based on Acoustic Emission and AdaBoost Algorithm

Li Ai 1[a], Vafa Soltangharaei 2[a], Paul Ziehl 3[a], Michel van Tooren 4[b] *

[a] *Department of Civil and Environmental Engineering, University of South Carolina, Columbia, SC, 29201, USA*
[b] *Collins Aerostructures, Chula Vista, CA, 91910, USA*

* *Corresponding author. Tel.: +01-803-777-9816; email: michael.vantooren@collins.com*

ABSTRACT

Impact is a substantial threat to the structural integrity of commercial and military aircraft components, and reliable evaluation of impact damage is therefore important for maintenance. Traditional impact detection for aircraft is based on scheduled visual inspection, intermittently followed by more comprehensive and detailed inspections. This approach is time consuming and detection may be subject to human error. This paper discusses a step in the development of a health monitoring system to automatically recognize and localize impact damage. One challenge to accomplish this goal is to minimize the number of sensors involved while still effectively localizing the zones of impact with an acceptable level of certainty. An artificial neural network and AdaBoost algorithm approach were employed to localize impact on an aircraft elevator having a thermoplastic composite surface, and results are compared and discussed.

Keywords: *Acoustic emission, Source localization, AdaBoost*
Article history: *Received ; Published .*

1. Introduction

Aircraft components may be subjected to impact damage caused by debris and hail during operation. The conventional approach to impact damage evaluation is based on visual inspection followed by more detailed nondestructive evaluation as needed. This approach is time consuming and prone to human error. A health monitoring system can be applied during operation to automate the recognition and localization of impact damage, either in addition to or as a partial replacement for visual inspection, due to recent advances in sensing technology and data analysis methods.

Acoustic emission (AE) is a structural health monitoring method of interest due to its extreme sensitivity to damage propagation in composite materials [1-11]. Several researchers have explored AE for fiber composite material [12-16]. For example, Marec et al [12] investigated the identification of damage in composite materials, where AE monitoring was employed during the three-point bending test on a fiber composite specimen. Several parametric features were extracted from the signals and those features were utilized for clustering through unsupervised pattern recognition with reasonable correlation observed between damage mechanics of the composite specimen and the clustering result. Liu et al. [13] used AE to study the failure and damage evolution of carbon fiber/epoxy composite laminates, where AE signals were collected during tensile testing and compared with the results provided by scanning electron microscopy (SEM). The study indicated that the failure modes of the carbon fiber/epoxy composite laminates including the fiber/matrix interface debonding, breakage and delamination, splitting matrix cracking, and fiber pull-out could be reasonably identified by the signals recorded. Whitlow et al. [14] developed a method to associate the final failure in continuous fiber reinforced ceramic matrix composites (CMCs) with AE signals recorded during in situ monitoring while digital image correlation (DIC) was implemented to obtain the surface strain measurements, with reasonable agreement found between the two methods. Saidane et al. [15] studied the evaluation of damage mechanisms during tensile tests in hybrid flax-glass fiber reinforced epoxy composites. The results from AE monitoring were compared with the results from SEM, and the authors presented the conclusion that the cumulative AE energy could indicate the overall failure of the composite. Khamedi et al. [16] worked on the identification of failure mechanisms of unidirectional carbon/epoxy composites, where the recorded signals were converted to wavelets and compared with SEM observations. The results of this study demonstrated that the results obtained with the transformed wavelet approach were in agreement with damage mechanisms observed in unidirectional carbon/epoxy composites.

AE has likewise been explored for characterization of damage due to impact on fiber composite materials [17-18]. Mal et al. [17] utilized AE to detect low velocity impact on graphite epoxy composite plates. The response of the plate was approached through modified lamination theory to obtain the detailed information on the relationship between the impact load and the signals. The results indicated that the occurrence of an impact loading can be easily detected from AE signals and delamination damage can be determined by analyzing the waveforms of the recorded AE signals. Saeedifar et al. [18] monitored damage initiation and growth in carbon epoxy laminates under quasi-static indentation and low velocity impact using several AE sensors. They concluded that AE is a powerful method to detect the

creation and growth of barely visible impact damage (BVID) in composite materials.

While the aforementioned indicates promise for the approach, one of the well understood challenges with AE monitoring is the collection of unwanted data and related to this discrimination between data associated with impact and other sources. This challenge is amplified for aircraft applications wherein a minimal number of sensors are allowed due to power and weight restrictions. Challenges therefore exist with localization of impacts in complex structures, such as an aircraft elevator. Machine learning algorithms are therefore investigated as a means to achieve reliable localization of impact events with a minimal number of sensors.

Artificial neural networks (ANN) have been explored in the past and are a form of artificial intelligence [19-29]. In previous work, Soltangharaei et al. [30] proposed a system to localize impact on aircraft components using AE. AE features were utilized as inputs to the ANN and source localization results were obtained as outputs. The results demonstrated that the impact localization using AE and ANN has the capability to provide reasonable localization results while satisfying weight and power restrictions. However, in this work only 100 AE signals were collected during the experiment and the specimen was divided into three zones for localization.

In the current study, improved impact detection is explored based on prior work [30]. A larger amount of AE signals was recorded during impacts in a laboratory environment and the specimen was divided into more zones. AdaBoost is a machine learning model based on boosting method [31]. The efficiency of the impact source localization approach using AdaBoost was investigated and compared with the localization approach using ANN. Results show that the impact monitoring system using AE and AdaBoost has a higher accuracy in locating the impact when compared to ANN.

2. Theoretical Background

The procedures in the proposed system include the in-flight and after-flight phases. The different steps of the in-flight/on-board detection and after-flight/off-board analysis is identified in the flowchart shown in Figure 1.

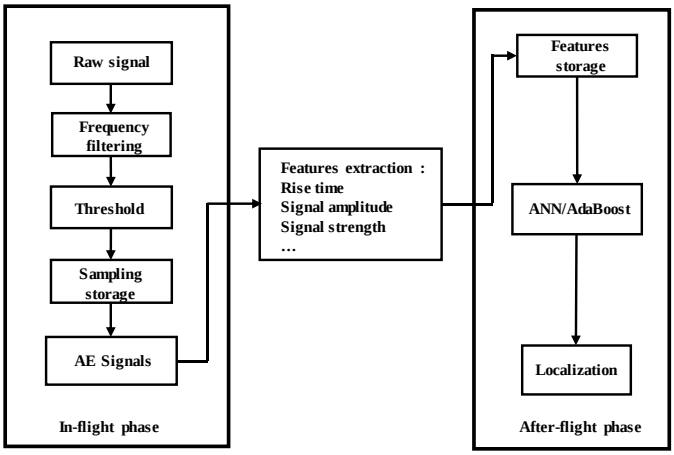

Figure 1. Procedures for smart impact detection system

In the in-flight phase, the initial signals received by the AE sensor are analog which can be analyzed after sampling and processing. The analog AE sensor signal is first passed through a hardware bandpass filter. Then, the analog signals are sampled and converted from analog to digital. Further processing of the signal is dependent upon a settable threshold for the signal amplitude. Processed signals are stored in the system after sampling. The stored signals are used on the ground in the after-flight phase to localize impact events. Several parametric AE features are extracted from the stored signals, with some details about the AE features described in Section 4. Feature storage after extraction is utilized as the input for machine learning models for source localization. In this paper, ANN and AdaBoost are explored.

3. Methodology

3.1. Acoustic emission

AE is a physical phenomenon related to stress waves generated by the rapid release of elastic energy when cracks or damage are formed in materials [32-33]. By attaching AE sensors to the surface of an object AE signals can be detected and recorded. The technique of collecting and analyzing AE signals to diagnose the status of an object is referred to as AE monitoring [34]. By processing the AE signal, different AE features can be extracted. Schematic representations of commonly used AE features such as "Amplitude", "Counts", "Energy", "Rise time" and "Duration" are shown in Figure 2.

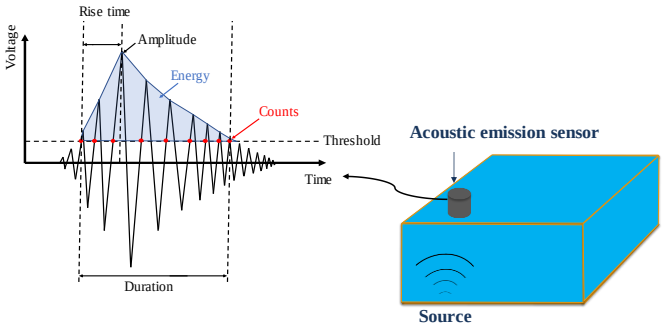

Figure 2. Schematic of acoustic emission approach

3.2. Back-propagation artificial neural network (BP-ANN)

The neural network adopted in the current work is a back-propagation artificial neural network (BP-ANN), which is one of the most popular techniques in the field of ANN [35]. It consists of an input layer, several hidden layers, and an output layer [36]. In each layer, there are multiple processing elements, called the neurons. Each of the neurons is connected to all others in the adjacent layers [37]. The number of neurons in the input layer and the output layer corresponds to the number of input variables and the dimension of the outputs [38].

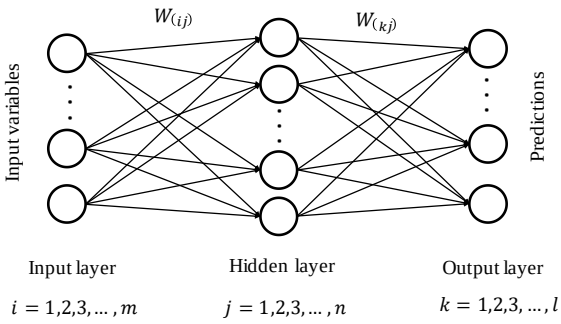

Figure 3. Three-layer artificial neural network

Figure 3 shows a typical three-layer artificial neural network consisting of layer i, j, and k. The number of neurons is m for layer i, n for layer j and l for layer k. $W_{(ij)}$ and $W_{(kj)}$ are the weights between the neurons in adjacent layers. The values of m and l are

related to the problem for solving, and n is determined by the network designer.

The calculation of a BP network consists of feedforward calculations and error backward calculations. In feedforward calculations, the input layer neurons receive the processed data, and the weighted sum corresponding to each neuron in the next layer is obtained by Eq. (1):

$$net_{(i)} = \sum_{j=1}^{n} W_{(ij)} \cdot O_{(j)} \quad (1)$$

Where, net is the net input of the i-th neuron, $W_{(ij)}$ is the weight, and $O_{(j)}$ is the output of the j-th neuron.

The output of the i-th neuron is obtained by submitting the weighted sum to the activation function, which can be linear, non-linear, or a unit step function. The S-type activation function, which is usually used to describe the nonlinearity of the system, is expressed in Eq. (2):

$$O_{(i)} = f\left[net_{(i)}\right] = \frac{1}{1+e^{-net_{(i)}}} \quad (2)$$

Where, $O_{(i)}$ is the output of the i-th neuron.

The result obtained by the output layer will be utilized to generate an error. The error E is defined as shown in Eq. (3):

$$E = \frac{1}{2}\sum_{j=1}^{l}[d_{(k)} - O_{(k)}]^2 \quad (3)$$

Where, $d_{(k)}$ is the label value. Labels refers to the informative tags of the corresponding input. $O_{(k)}$ is the prediction value in the k-th neuron of output layer.

To modify the weights to obtain more accurate results, the error of the output layer will be back propagated to the previous adjacent layer using the gradient descent method, and finally propagated to the input layer. The value of the weight change is obtained by Eq. (4):

$$\Delta W_{(kj)} = -\alpha \frac{\partial E}{\partial W_{(kj)}} \quad (4)$$

Where, α is learning rate which adjusts the amplitude of the weight change.

All the connection weights are assigned with random values initially, and then modified according to the results of the BP training process. The overall procedure is presented in Figure 4.

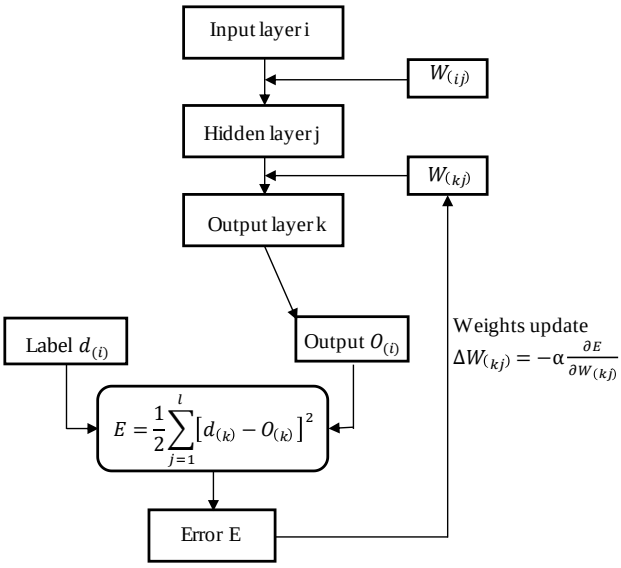

Figure 4. Mechanism of a BP network

3.3. AdaBoost algorithm

The Boosting algorithm is an integrated learning technique that can enhance several weak learning models with a prediction accuracy that is only slightly higher than the random guess to a strong model with high prediction accuracy [31]. In the case where it is very difficult to directly construct a strong learning model, it provides an effective method for the design of learning algorithms. AdaBoost is the abbreviation of "Adaptive Boosting". AdaBoost is adaptive in the sense that subsequent weak learners are tweaked by weight in favor of those instances misclassified by previous leaners. Each weak model inside the AdaBoost obtains a function through repeated iterations. At the end of the iterations, a weight is assigned to each weak function. The strong prediction function is weighted by the weak functions [39].

In this paper, the decision tree was utilized as a weak learning model in the AdaBoost classification. Assuming the training dataset is an N dimensional set $D = \{(X_1, y_1), (X_2, y_2), (X_3, y_3) \ldots (X_N, y_N)\}$, X_i refers to the ith input data, y_i refers to the category of the ith input. Each input data which has k features is a k dimensional vector $\{x^1, x^2, x^3 \ldots x^k\}$. The classification threshold of the ith feature in one input v_i can be provided by Eq. (5):

$$v_i = \min(x^i) + j * s \quad (5)$$

Where, i= 1, 2, …, k, j= -1, 0, 1, 2…, 10. s refers to the step size which can be calculated by Eq. (6):

$$s = \frac{1}{10}[(\max(x^i) - min(x^i)] \quad (6)$$

A decision tree can be constructed based on the classification threshold of each feature in the input data. The procedure of the decision tree is shown in Figure 5. The decision tree with the lowest error is selected as the optimized tree $T(x)$ that is implemented in the AdaBoost model.

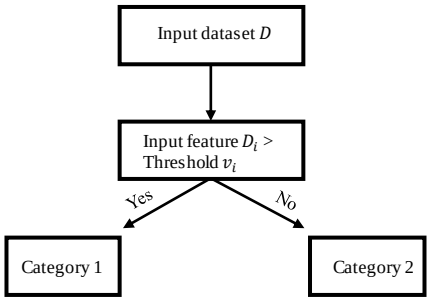

Figure 5. Mechanism of a decision tree

An initial weight set W is assigned to the AdaBoost model: $W = (W_1, W_2, W_3, \ldots, W_N)$. Every element in the weight set has the same initial weight $1/N$.

Assuming there are M decision trees in the AdaBoost model. The error of the mth decision tree can be obtained by Eq. (7)

$$\varepsilon_m = \sum_{i=1}^{N} W_{mi}, T_m(X_i) \neq y_i \quad (7)$$

Where, W_m refers to the initial weight of the mth decision tree.

The updated coefficient α_m can be calculated by Eq. (8):

$$\alpha_m = \frac{1}{2}\ln\left(\frac{1-\varepsilon_m}{\varepsilon_m}\right) \quad (8)$$

The updated weight W_{m+1} for the next decision tree T_{m+1} can be provided by Eq. (9) and Eq. (10):

$$W(correct)_{m+1i} = \frac{W_{mi}}{Z_m} e^{-\alpha_m} \quad (9)$$

$$W(wrong)_{m+1i} = \frac{W_{mi}}{Z_m} e^{\alpha_m} \quad (10)$$

Where, $W(correct)$ refers to the weight assigned to the input data that was correctly classified by the last decision tree. $W(wrong)$ refers to the weight assigned to the input data that was classified by mistake. Z_m is the normalization factor, which can be calculated by Eq. (11).

$$Z_m = sum(W_m) \quad (11)$$

The procedural flow of the AdaBoost model utilized in this paper is shown in Figure 6. AE parametric features are extracted from the AE signals and implemented as input. The final localization result is given by the model after the iterations of M decision trees. The influence of the number of decision trees is discussed in Section 5.

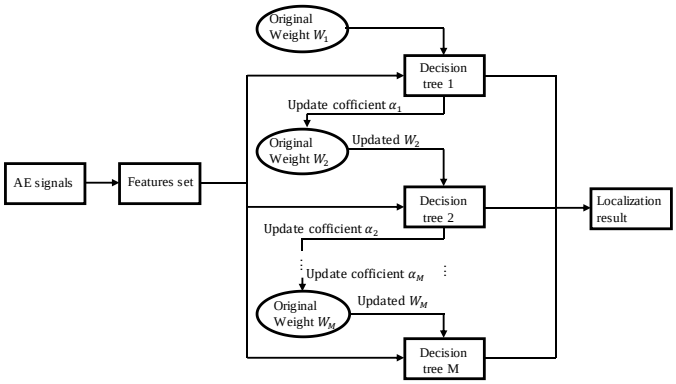

Figure 6. The mechanism of the AdaBoost model

4. Experiment

4.1. Steel sphere impact experiment

A steel sphere impact experiment was conducted on an aircraft elevator to validate the impact detection system proposed in this paper. The elevator was mounted on a steel frame made of 5-inch channels with an overall length of 6.10 meters and a height of 0.61 meters. The hinge brackets on the elevator spar were connected to hinge points located on the frame. The impact experiment was conducted using a steel sphere of 0.013 meters in diameter. The weight of the steel sphere is 8.40 grams. The drop height of the steel sphere was kept constant at 0.61 meters for all the impacts (Figure 7). The impact energy of the steel sphere is 0.05 J. A guide tube was used to control the location and height of each impact. The size and material of the impactor and the drop height were control constantly. The only varying variable during this study was the locations of impact.

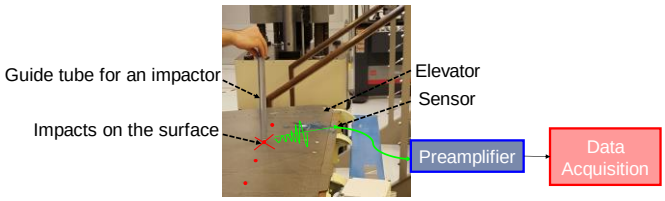

Figure 7. Steel sphere drop test

There are 20 ribs in the elevator. Figure 8 shows the layout of the ribs in the elevator. Three locations were marked on each rib. The impact locations are shown in Figure 8 and marked as red points. Each location was impacted 60 times by the steel sphere. A PAC Micro-30 AE sensor was attached to the front spar of the elevator as shown in the Figure.

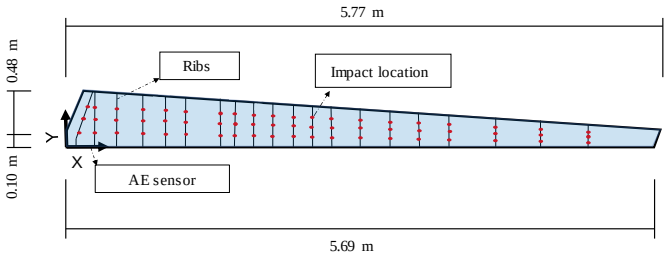

Figure 8. Impact and sensor locations

4.2. Acoustic Emission Instrumentation and Setup

The hardware and software of the AE system were produced by the Mistras Group Inc., Princeton Junction, New Jersey. AE signals were acquired by a 16-channel DiSP system. The pre-trigger time, which recovers AE waveforms before the threshold crossing, was defined as 256 µs. The sampling rate was 5MHz (or 5,000,000 samples per second). The duration was set to 10,000 µs. The peak definition time, which means the time from threshold crossing to peak amplitude, was defined as 200 µs and the hit definition time, which determines the stop point of recording, was set to 400 µs. This is typically twice the peak definition time [40]. The hit lockout time, which prevents recording late-arriving signals and reflected hits, was set to 400 µs.

5. Results and Discussion

5.1. Define zones

In this paper, the source localization of AE events was considered as the classification problem. The AE signals are classified to their corresponding zones. Five scenarios were taken into consideration. In scenario 1, the elevator surface was divided into 2 zones with each zone having 10 ribs.

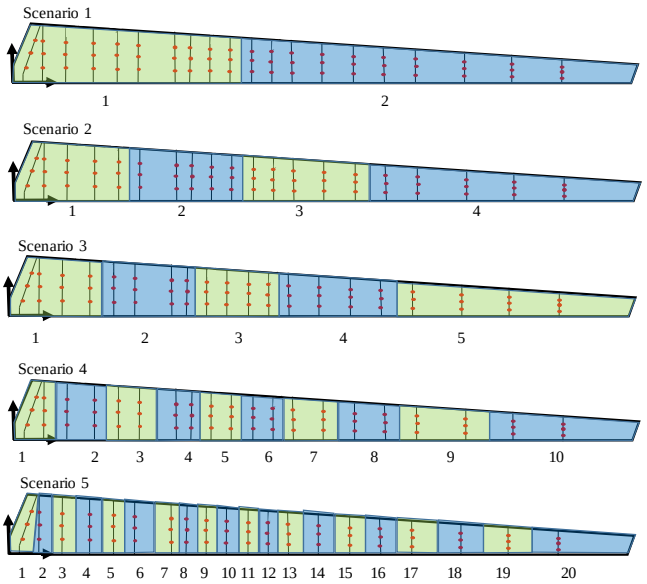

Figure 9. Five scenarios of zonal division

In scenario 2, all ribs on the surface were divided into 4 zones, with 5 ribs in each zone. In scenario 3, 5 zones were considered, each zone having 4 ribs. In scenario 4, the elevator surface was

divided into 10 zone with each zone having 2 ribs. In scenario 5, the elevator surface was divided into 20 zones, with each zone having 1 rib. The 5 scenarios of zonal division are presented in Figure 9. The zonal divisions were utilized as labels of the ANN and AdaBoost models.

5.2. Input preparation

During the impact experiment 3,600 AE signals were collected. Feature extraction was conducted on the AE events. The AE signals after extraction contain 15 features: "Amplitude", "Counts", "Rise time", "Duration", "Average frequency", "Root mean square", "Average signal level", "Energy", "Absolute energy", "Peak frequency", "Reverberation frequency", "Initial frequency", "Signal strength", "Frequency centroid" and "Counts to peak". The feature-based dataset was implemented as training, validation, and testing in the ANN and AdaBoost models.

5.3. Results of source localization using BP-ANN

The dataset with 15 features was assigned to the BP-ANN as input. Ratios for training, validation, and testing datasets were 3:1:2. In the 3,600 data signals, 1,800 of them were randomly selected and assigned as training data, 600 were randomly selected as validation data, and 1,200 were randomly selected as testing data. A trial-and-error test was conducted for ANN model configuration selection for scenario 1 (two zones), with the zonal division in scenario 1 was utilized as the label. One commonly used method in determining the number for neurons in hidden layers is:

$$N_{hidden} \leq 2N_{input} + 1 \quad (12)$$

Where, N_{hidden} is the number of neurons in the hidden layers and N_{input} is the number of input features.

According to Eq. (12) the maximum number of neurons is 31. An ANN with 1 hidden layer and an ANN with 2 hidden layers were tested while the neuron number of each layer was increased from 1 to 31. The test was repeated 100 times, with the averaged results provided in Figure 10. The highest accuracy (97.6%) is obtained when the configuration of ANN is two hidden layers with 26 neurons for each of the hidden layers. Therefore, two hidden layers with 26 neurons for each hidden layer was selected as the configuration of the ANN for AE source localization.

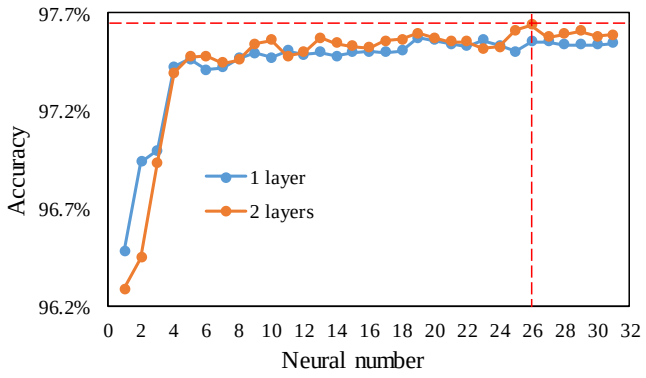

Figure 10. Trial and error results

The localization of AE in scenario 1 (two zones) was repeated 100 times. The averaged accuracy is 97.6% (Figure 10). The performance curve is provided in Figure 11a, with the least cross-entropy for validation found in epoch 27. Therefore, the training process was stopped at epoch 27 and tested on the testing data. The classification results are shown in the confusion matrix (Figure 11b). The numbers of AE signals successfully classified in their corresponding zones are shown in the main diagonal of the confusion matrix. In all the 1,200 test signals, there were 1,171 AE signals correctly located in the corresponding zone, with accuracy was 97.6%. 583 signals in zone 1 were correctly localized while the remaining 19 signals were assigned to zone 2 by mistake. 588 signals in zone 2 were successfully classified to zone 2 while the remaining 10 signals were mistakenly localized to zone 1. The recall rate and precision of zone 1 are respectively 96.8% and 98.3%, The recall rate and precision of zone 2 are 98.3% and 96.9%.

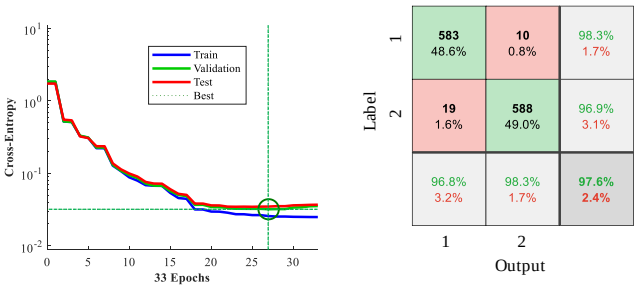

(a) (b)

Figure 11. The performance of ANN in scenario 1: a) performance curve; b) confusion matrix of ANN

The AE source localization approach using ANN was also tested on scenario 2, 3, 4, and 5. The highest localization accuracy (97.6%) was observed in scenario 1. As expected, the accuracy decreases with increasing zone number. The accuracies were 93.5% in scenario 1, 88.2% in scenario 3, and 81.8% in scenario 4. The lowest accuracy was obtained in scenario 5 with the elevator divided into 20 zones. In all of the five scenarios. The dominant misclassification was on the neighboring rib. It should be notice that the concept of overlapping [29] was not applying in this study to reduce error. The comparison between various scenarios and different localization methods was made based on the same condition without considering overlap.

5.4. Results of source localization using AdaBoost

The data used for the training of this model was the same as that used for the ANN. In the 3,600 data signals, 2,400 were randomly selected for training. Five-fold cross validation was applied in the training process. The remaining 1,200 were implemented for testing. The influence of the number of trees inside the AdaBoost model was studied. The zonal division in all five scenarios were utilized as labels. The AdaBoost model was tested with tree numbers varying from 1 to 500, with an interval of 50. The results of scenario 1 (2 zones) are shown in Figure 12a. The accuracy increases rapidly when the number of trees increases from 1 to 150. The trend turns flat when the number of trees grows from 150 to 500. The highest accuracy (99.2%) can be observed when the AdaBoost model has 400, 450 and 500 trees.

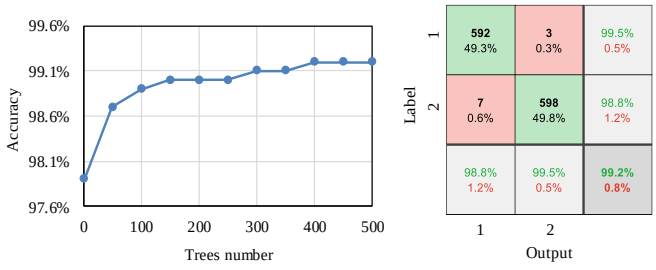

(a) (b)

Figure 12. The performance of AdaBoost in scenario 1: a) accuracies of AdaBoost when tree number increases from 1 to 500, b) confusion matrix of AdaBoost with 500 trees

Source localization using the AdaBoost model with 500 trees in scenario 1 was repeated 100 times. Figure 12b shows the localization. The model can successfully localize 1,171 AE data signals to their corresponding zone. To be more specific, the number of the AE data that were correctly localized in the corresponding zones is respectively 592 in zone 1 and 598 in zone 2. The recall rate and precision of zone 1 are respectively 98.8% and 99.5%, The recall rate and precision of zone 2 are 99.5% and 98.8%.

AE source localization using AdaBoost was also tested on scenarios 2, 3, 4, and 5. The results of all five scenarios are shown in Figure 13. The curves of accuracy versus tree number for the five scenarios reveal a similar trend. An obvious increase can be observed when tree number grows from 1 to 150. No obvious change of accuracy can be observed when the number of trees continually increases to 500. The highest localization accuracies are 96.5% for scenario 2, 94.2% for scenario 3, 89.9% for scenario 4, and 78.9% for scenario 5.

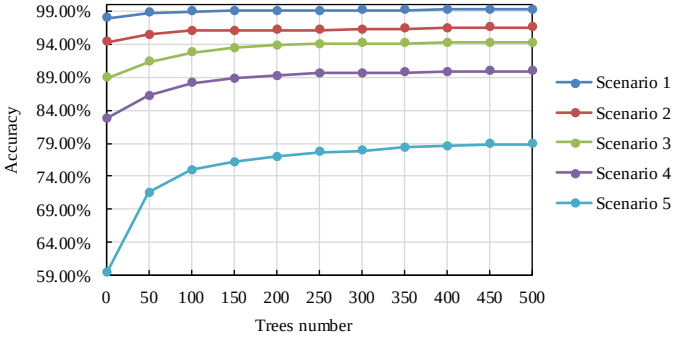

Figure 13. Accuracies of AdaBoost model for all scenarios

5.5. Discussion

The effect of zone number was investigated. In scenario 1 when the elevator was divided into two zones, the AdaBoost model with 500 decision trees resulted in the highest accuracy (99.2%). The AdaBoost model with one tree, which can be considered as the decision tree without boosting, resulted in accuracy of 97.9%. The lowest accuracy (97.6%) was obtained by the BP-ANN model. In scenario 2 when the elevator was divided into four zones, the highest accuracy (96.5%) was acquired by the AdaBoost model with 500 decision trees. The AdaBoost model with one tree resulted in accuracy of 94.3%, while the BP-ANN model resulted in the lowest accuracy of 93.5%. In scenario 3 with four zones, the highest accuracy (94.2%) was observed when the AdaBoost model with 500 decision trees was utilized. The accuracy of the AdaBoost model with one tree was 88.9%. The lowest accuracy (88.2%) was provided by the BP-ANN model. In scenario 4 when the elevator was divided into four zones, the sequence was the same as scenario 1, 2, and 3. The accuracy (89.8%) of the AdaBoost model with 500 trees resulted in the highest accuracy. The AdaBoost model with one tree resulted in accuracy of 82.8%. The lowest accuracy (81.6%) was obtained by the BP-ANN model. In scenario 5 when the elevator was divided into four zones, the sequence was changed. The accuracy of the AdaBoost model with 500 remains the highest (78.9%), however, the BP-ANN model acquired an accuracy (64.8%) higher than the accuracy (59.5%) of AdaBoost with one tree.

The curves of accuracy versus zone number are plotted in Figure 14. The accuracies of the three models decrease with more zones as expected. The AdaBoost model with 500 trees has the highest accuracy in every scenario. A very high accuracy close to 100% was observed for the case of two zones, but it did not offer much improvement as there are 10 ribs in each zone. Human effort is still needed to identify which rib was impacted. The localization accuracy (78.9%) is low when the elevator was divided into 20 zones. A relatively high accuracy (89.9%) is obtained when the elevator is divided into10 zones, with only two ribs in each zone. Human effort and human error would be substantially reduced through identifying impacts from two ribs.

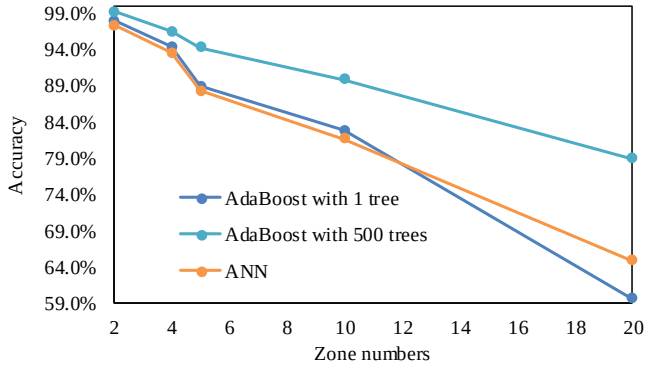

Figure 14. Influence of zone number

Computing time is another factor to consider and evaluate for automated source localization. The localization accuracy and the computing time for training and testing of the BP-ANN and AdaBoost model with 500 trees are presented in Table 1. The computing process requires more time as the number of zones increases. In scenario 4 with ten zones, the training time for the ANN and the AdaBoost model with 500 trees were 2.6 seconds and 26.1 seconds, clearly indicating the BP-ANN requires much less time to train a model. The computing time for the well-trained model to provide the localization results based on testing input was similar for both approaches, with 0.2 seconds for the BP-ANN, and 0.3 seconds for AdaBoost with 500 trees.

Table 1. Accuracies and **c**omputing times of BP-ANN and AdaBoost in different scenarios

Scenario	Approach	Accuracy	Training time (s)	Testing time (s)
1	BP-ANN	97.6%	1.1	0.1
	AdaBoost	99.2%	14.1	0.2
2	BP-ANN	93.5%	1.3	0.1
	AdaBoost	96.5%	17.7	0.2
3	BP-ANN	88.2%	1.5	0.2
	AdaBoost	94.2%	21.4	0.3
4	BP-ANN	81.8%	2.1	0.2
	AdaBoost	89.8%	26.1	0.3
5	BP-ANN	64.8%	2.6	0.2
	AdaBoost	78.9%	32.2	0.4

For the application envisioned, the localization model will be trained with historical AE signals collected and labeled in the past and therefore computational time will not be a primary consideration. In the after-flight phase, source localization will be

conducted based on a trained model, meaning the testing time is the primary factor to consider. Therefore, the AdaBoost model which has higher accuracy and similar testing time is preferred over the ANN approach. Furthermore, the AdaBoost with 500 trees and division of the elevator into 10 zones appears to offer an optimum solution among those considered.

6. Conclusions

A smart impact detection system for a thermoplastic aircraft elevator component is proposed to automate and thereby improve upon traditional visual inspection. To verify the effectiveness of the proposed system, an impact experiment was conducted on a real-scale elevator specimen. The system consists of a single AE sensor, associated cabling, and small onboard computing system. Acoustic emission signals were captured during the impact experiments. A BP-ANN model and AdaBoost model were utilized to localize the impact in five zonal division scenarios and results were compared. The influence of the number of zones and the number of decision trees in the AdaBoost model was explored.

Pertinent conclusions are:

1. Compared to the BP-ANN, improved performance was observed for impact detection and localization in all five zonal division scenarios when the AdaBoost model was employed.
2. A significant increase of localization accuracy was observed when the number of decision trees inside the AdaBoost model increased from 1 to 150. When the number of trees increased to 500, the accuracy converged. The optimized number of decision trees for AdaBoost was found to be 500.
3. The zonal division significantly influences localization accuracy. Both the BP-ANN and the AdaBoost model show a decay of accuracy when the zone number was increased from two to 20. When the elevator was divided into 10 zones, an acceptable localization accuracy was achieved from the AdaBoost model with 500 trees (89.9%). Comparing BP-ANN and AdaBoost, computing time required for the well-trained model is similar. With consideration to accuracy and computing time, dividing the elevator into 10 zones and using AdaBoost with 500 trees appears to be the optimum approach for impact source localization in this application.

Further work could be an investigation of the effect of impact energy, and impactor material. The advanced deep learning algorithms like deep belief networks and convolutional neural networks could be applied to this system.

Acknowledgments

This paper is based upon work partially supported by GKN - Fokker Aerostructures BV.

7. References

1. Ono, K. (2011). Application of acoustic emission for structure diagnosis. Diagnostyka, 3-18. Aiordachioaie D., R., Teodorescu R.,
2. Li, W., Xu, C., Ho, S. C. M., Wang, B., & Song, G. (2017). Monitoring concrete deterioration due to reinforcement corrosion by integrating acoustic emission and FBG strain measurements. Sensors, 17(3), 657.
3. Y., Bao, J., Poddar, B., & Giurgiutiu, V. (2018). Toward identifying crack-length-related resonances in acoustic emission waveforms for structural health monitoring applications. Structural Health Monitoring, 17(3), 577-585.
4. Soltangharaei, V., Anay, R., Hayes, N. W., Assi, L., Le Pape, Y., Ma, Z. J., & Ziehl, P. (2018). Damage mechanism evaluation of large-scale concrete structures affected by alkali-silica reaction using acoustic emission. Applied Sciences, 8(11), 2148.
5. Abdelrahman, M., ElBatanouny, M., Dixon, K., Serrato, M., & Ziehl, P. (2018). Remote Monitoring and Evaluation of Damage at a Decommissioned Nuclear Facility Using Acoustic Emission. Applied Sciences, 8(9), 1663.
6. Anay, R., Soltangharaei, V., Assi, L., DeVol, T., & Ziehl, P. (2018). Identification of damage mechanisms in cement paste based on acoustic emission. Construction and Building Materials, 164, 286-296.
7. Soltangharaei, V., Anay, R., Assi, L., Ziehl, P., & Matta, F. (2018). Damage identification in cement paste amended with carbon nanotubes. AIP Conference Proceedings (Vol. 1949, No. 1, p. 030006). AIP Publishing LLC.
8. Ai, L., Greer, B., Hill, J., Soltangharaei, V., & Ziehl, R. A. P. (2019). Finite element modeling of acoustic emission in dry cask storage systems generated by cosine bell sources. AIP Conference Proceedings (Vol. 2102, No. 1, p. 130001). AIP Publishing LLC.
9. Anay, R., Lane, A., Jáuregui, D. V., Weldon, B. D., Soltangharaei, V., & Ziehl, P. (2020). On-Site Acoustic-Emission Monitoring for a Prestressed Concrete BT-54 AASHTO Girder Bridge. Journal of Performance of Constructed Facilities, 34(3), 04020034.
10. Soltangharaei, V., Anay, R., Ai, L., Giannini, E. R., Zhu, J., & Ziehl, P. (2020). Temporal Evaluation of ASR Cracking in Concrete Specimens Using Acoustic Emission. Journal of Materials in Civil Engineering, 32(10), 04020285.
11. Ai, L., Soltangharaei, V., Anay, R., van Tooren, M. J., & Ziehl, P. (2020). Data-Driven Source Localization of Impact on Aircraft Control Surfaces. 2020 IEEE Aerospace Conference (pp. 1-10). IEEE.
12. Marec, A., Thomas, J. H., & El Guerjouma, R. (2008). Damage characterization of polymer-based composite materials: Multivariable analysis and wavelet transform for clustering acoustic emission data. Mechanical systems and signal processing, 22(6), 1441-1464.
13. Liu, P. F., Chu, J. K., Liu, Y. L., & Zheng, J. Y. (2012). A study on the failure mechanisms of carbon fiber/epoxy composite laminates using acoustic emission. Materials & Design, 37, 228-235.
14. Whitlow, T., Jones, E., & Przybyla, C. (2016). In-situ damage monitoring of a SiC/SiC ceramic matrix composite using acoustic emission and digital image correlation. Composite Structures, 158, 245-251.
15. Saidane, E. H., Scida, D., Assarar, M., & Ayad, R. (2017). Damage mechanisms assessment of hybrid flax-glass fibre composites using acoustic emission. Composite Structures, 174, 1-11.
16. Khamedi, R., Abdi, S., Ghorbani, A., Ghiami, A., & Erden, S. (2019). Damage characterization of carbon/epoxy composites using acoustic emission signals wavelet analysis. Composite Interfaces.
17. Mal, A. K., Shih, F., & Banerjee, S. (2003). Acoustic emission waveforms in composite laminates under low velocity impact. Smart Nondestructive Evaluation and Health Monitoring of Structural and Biological Systems II (Vol. 5047, pp. 1-12). International Society for Optics and Photonics.
18. Saeedifar, M., Najafabadi, M. A., Zarouchas, D., Toudeshky, H. H., & Jalalvand, M. (2018). Barely visible impact damage assessment in laminated composites using acoustic emission. Composites Part B: Engineering, 152, 180-192.
19. Sarle, W. S. (1994). Neural networks and statistical models.
20. Hassoun, M. H. (1995). Fundamentals of artificial neural networks. MIT press.
21. Yao, X. (1999). Evolving artificial neural networks. Proceedings of the IEEE, 87(9), 1423-1447.
22. Yegnanarayana, B. (2009). Artificial neural networks. PHI Learning Pvt. Ltd.
23. Zhang, G., Patuwo, B. E., & Hu, M. Y. (1998). Forecasting with artificial neural networks: The state of the art. International journal of forecasting, 14(1), 35-62.
24. Gardner, M. W., & Dorling, S. R. (1998). Artificial neural networks (the multilayer perceptron)—a review of applications in the atmospheric sciences. Atmospheric environment, 32(14-15), 2627-2636.
25. Basheer, I. A., & Hajmeer, M. (2000). Artificial neural networks: fundamentals, computing, design, and application. Journal of microbiological methods, 43(1), 3-31.

26. Priddy, K. L., & Keller, P. E. (2005). Artificial neural networks: an introduction (Vol. 68). SPIE press.
27. Graupe, D. (2013). Principles of artificial neural networks (Vol. 7). World Scientific.
28. Amato, F., López, A., Peña-Méndez, E. M., Vaňhara, P., Hampl, A., & Havel, J. (2013). Artificial neural networks in medical diagnosis.
29. Van Gerven, M., & Bohte, S. (2017). Artificial neural networks as models of neural information processing. Frontiers in Computational Neuroscience, 11, 114
30. Soltangharaei, V., Anay, R., Begrajka, D., Bijman, M., ElBatanouny, M. K., Ziehl, P., & Van Tooren, M. J. (2019). A minimally invasive impact event detection system for aircraft movables. AIAA Scitech 2019 Forum (p. 1268).
31. Rätsch, G., Onoda, T., & Müller, K. R. (2001). Soft margins for AdaBoost. Machine learning, 42(3), 287-320.
32. Wadley, H. N. G., & Mehrabian, R. (1984). Acoustic emission for materials processing: a review. Materials Science and Engineering, 65(2), 245-263.
33. Grosse, C. U., & Ohtsu, M. (Eds.). (2008). Acoustic emission testing. Springer Science & Business Media.
34. Scruby, C. B. (1987). An introduction to acoustic emission. Journal of Physics E: Scientific Instruments, 20(8), 946.
35. Hecht-Nielsen, R. (1992). Theory of the backpropagation neural network. In Neural networks for perception (pp. 65-93). Academic Press.
36. Wang, J. Z., Wang, J. J., Zhang, Z. G., & Guo, S. P. (2011). Forecasting stock indices with back propagation neural network. Expert Systems with Applications, 38(11), 14346-14355.
37. Tsai, C. P., & Lee, T. L. (1999). Back-propagation neural network in tidal-level forecasting. Journal of Waterway, Port, Coastal, and Ocean Engineering, 125(4), 195-202.
38. Erb, R. J. (1993). Introduction to backpropagation neural network computation. Pharmaceutical research, 10(2), 165-170.
39. Schapire, R. E. (2013). Explaining adaboost. Empirical inference (pp. 37-52). Springer, Berlin, Heidelberg.
40. Laksimi, A., Benmedakhene, S., & Bounouas, L. (1999). Monitoring acoustic emission during tensile loading of thermoplastic composites materials. Proceeding of ICCM (Vol. 12)